**Naval Oceanographic Office**

Stennis Space Center
MS 39522-5001

Technical Note
TN 03-93
May 1993



TN 03-93

# OPTICAL PROPERTIES OF THE RED SEA



Prepared under the authority of
**Commander,**
**Naval Oceanography Command**



This technical note has been prepared as part of a transition product between the Naval Research Laboratory (NRL) and the Naval Oceanographic Office (NAVOCEANO). This program's effort provides NAVOCEANO development capability of an ocean color optical database. It is intended to show the influence of the monsoonal regimes on the ocean color signature of the Red Sea.

RELEASED FOR PUBLICATION

Thomas L. Sandidge Jr

THOMAS L. SANDIDGE
Branch Head
Satellite Analysis and Data
Fusion Branch

David L. Martin

CDR DAVID L. MARTIN
Director
Warfighting Support Center

R Bandt acting

CDR D. J. WHITFORD
Director
Warfighting Support Directorate

# DISCLAIMER NOTICE

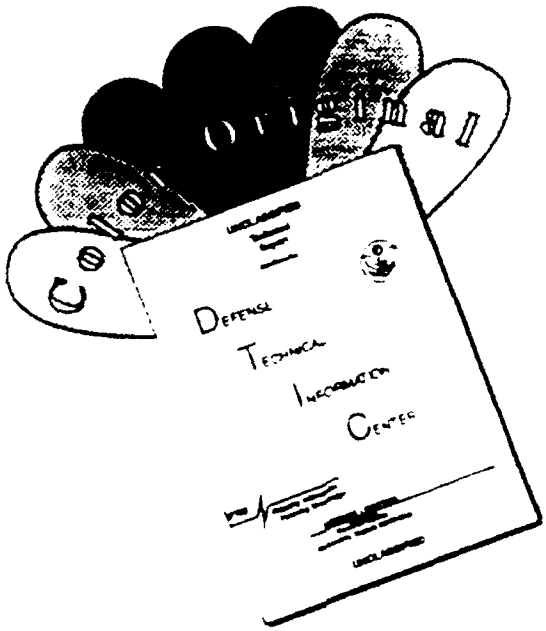


THIS DOCUMENT IS BEST QUALITY AVAILABLE. THE COPY FURNISHED TO DTIC CONTAINED A SIGNIFICANT NUMBER OF COLOR PAGES WHICH DO NOT REPRODUCE LEGIBLY ON BLACK AND WHITE MICROFICHE.

# REPORT DOCUMENTATION PAGE

*Form Approved*
*OMB No 0704-0188*



| 1. AGENCY USE ONLY *(Leave blank)* | 2. REPORT DATE | 3. REPORT TYPE AND DATES COVERED |
|---|---|---|
| | May 1993 | Technical Note |

**4. TITLE AND SUBTITLE**

OPTICAL PROPERTIES OF THE RED SEA

**5. FUNDING NUMBERS**

**6. AUTHOR(S)**

Christine M. Kirby, Michelle M. Parmeter,
Robert A. Arnone, and R.A. Oriol

**7. PERFORMING ORGANIZATION NAME(S) AND ADDRESS(ES)**

Commanding Officer
Naval Oceanographic Office
1002 Balch Blvd.
Stennis Space Center, MS 39522-5001

**8. PERFORMING ORGANIZATION REPORT NUMBER**

TN 03-93

**9. SPONSORING / MONITORING AGENCY NAME(S) AND ADDRESS(ES)**

Commander,
Naval Oceanography Command
1020 Balch Blvd.
Stennis Space Center, MS 39529-5005

**10. SPONSORING / MONITORING AGENCY REPORT NUMBER**

**11. SUPPLEMENTARY NOTES**

Prepared in cooperation with Naval Research Laboratory Detachment, Stennis Space Center and Planning Systems, Incorporated, Slidell, Louisiana

**12a. DISTRIBUTION / AVAILABILITY STATEMENT**

Approved for public release;
distribution is unlimited.

**12b. DISTRIBUTION CODE**

**13. ABSTRACT** *(Maximum 200 words)*

Optical properties of the Red Sea are characterized using the Coastal Zone Color Scanner (CZCS) for the period of January 1979 to December 1980. The ocean color imagery gathered by the CZCS is used to determine the diffuse attenuation coefficient, K, at 490 nm. The distribution of K(490) is shown to change spatially and temporally during the 2-year period. The Red Sea circulation is influenced by the monsoons which have significant effect on the surface optical properties. Optical properties of five different regions within the Red Sea are identified and statistics determined. The southern Red Sea exhibits a higher variability than the northern Red Sea. The K(490) optical properties were low during the summer months of June and July but showed a significant increase in November as a result of the onset of the Northeast monsoon. A strong interannual difference in K(490) between 1979 and 1980 is shown for the five Red Sea regions.

| 14. SUBJECT TERMS | 15. NUMBER OF PAGES |
|---|---|
| Optical properties, Monsoon regimes, Red Sea Circulation, CZCS data sets | 37 |
| | 16. PRICE CODE |

| 17. SECURITY CLASSIFICATION OF REPORT | 18. SECURITY CLASSIFICATION OF THIS PAGE | 19. SECURITY CLASSIFICATION OF ABSTRACT | 20. LIMITATION OF ABSTRACT |
|---|---|---|---|
| Unclassified | Unclassified | Unclassified | UL |

# OPTICAL PROPERTIES OF THE RED SEA

Christine M. Kirby[1], Michelle M. Parmeter[1], R.A. Arnone[2]
and R.A. Oriol[3]

[1]Naval Oceanographic Office
Warfighting Support Center
Stennis Space Center, Mississippi

[2]Naval Research Laboratory
Remote Sensing Group
Stennis Space Center, Mississippi

[3]Planning Systems, Incorporated
Slidell, Louisiana

TABLE OF CONTENTS



LIST OF FIGURES

LIST OF FIGURES (CON.)



LIST OF TABLES

Table

## Acknowledgements

The authors gratefully acknowledge the assistance of the following people: Charles McClain and Gary Fu of NASA, Goddard Space Flight Center, for the development and support of PC-SEAPAK software and processing; Gene Feldman for supplying NASA products of the Global CZCS data set; and Oceanographer of the Navy program manager, Kenneth Ferer, for support in the development of this project entitled "Coastal Optics Planner."

# I. INTRODUCTION

Satellite ocean color imagery from the Coastal Zone Color Scanner (CZCS) has clearly shown the global distribution of chlorophyll in the upper ocean (Feldman et al., 1989). The spatial scales of chlorophyll variability illustrated in the surface values were high and demonstrated that the surface biological distribution was much higher than originally thought (Yoder et al., 1987).

The ocean's optical environment has a similar scale of high variability. In Case 1 waters, where the biological distribution covaries with the optical properties (Morel and Prieur, 1977), global distributions of diffuse attenuation coefficient, K(490), are similar to that of chlorophyll (Austin and Petzold, 1981; Lewis et al., 1988). For the majority of the ocean environment, the chlorophyll distribution is the primary controlling factor of the diffuse attenuation coefficient. Coastal waters are also influenced by terrigenous material (suspended sediment and dissolved organics, i.e., *gelbstoff*), which has significant influence on the optical properties. In Case 2 waters, the optical variability is highly changeable and is responsive to different types of physical oceanographic forcing. The processes controlling the bio-optical environment on the ocean surface are believed to be strongly linked to physical processes. Understanding the interaction of these processes to predict the optical environment and identifying the scales of spatial and temporal optical variability can be greatly improved through the use of CZCS data (Arnone and LaViolette, 1991).

The Red Sea was selected to characterize the regional surface optical environment and its interaction with the monsoon seasons. The effect of monsoons was shown to increase significantly the optical properties in the Arabian Sea (Arnone and Oriol, 1990a). Within the Red Sea, the monsoon influence is not as strong as in the Arabian Sea; therefore, these seasonal trends were not expected to impact significantly the optical climate. The Red Sea is affected by different physical oceanographic and meteorological forces that produce changes in the surface and subsurface ocean structure throughout the entire sea. The Red Sea has different geographical provinces bounded by the bathymetry, physical circulation, and winds (Siedler, 1969). These changing conditions within these provinces should have significant influence on the bio-optical signature.

The objective of this report is to characterize the surface optical properties within the Red Sea and determine the seasonal significance of the monsoons. Monthly climatology of the surface optical properties will be examined for a 2-year period, 1979 to 1980, to define the temporal variability. Additionally, statistics of the optical properties occurring within different provinces will be compared to the controlling forces within the provinces. A comparison of how these individual provinces influence the total optical climate in the Red Sea will be addressed.

## II. OCEAN-ATMOSPHERE CONDITIONS IN THE RED SEA

The mean circulation of the Red Sea is driven mainly by thermohaline processes resulting from elevated evaporation at the surface in concert with the overall wind field (Siedler, 1969). Although the Red Sea is connected to the Mediterranean Sea by the Suez Canal, there is minimal exchange of water. The Strait of Bab al Mandab in the southern Red Sea (figure 1) is the primary exchange between the Red Sea and the Gulf of Aden. The real separation between waters of the Red Sea and those of the Gulf of Aden occurs at the Hanish Sill (100 m), where the channel is the shallowest and where considerable mixing takes place. The basic structure and circulation of the Red Sea water masses are perturbed by the effects of seasonal changes in evaporation and wind stress. Evaporation far exceeds precipitation in this region, and there is no river inflow; therefore, the water budget dictates a net inflow through the Strait of Bab al Mandab in response to the evaporative loss in the Red Sea Basin. The surface salinity of the Red Sea is high (approximately 40 ppt) because of this evaporation of fresh water. The density of this surface layer is elevated compared to the density of the adjacent Arabian Sea. A circulation pattern develops so that the less dense Arabian water flows on the surface through the Strait of Bab al Mandab, and the Red Sea water outflows, at depth, near the Hanish Sill (Siedler, 1969).

The basic circulation of the Red Sea is affected by marked seasonal variations of the wind field, which is controlled by the monsoon wind system. Over central Asia, during the Southwest (SW) monsoon, there is usually a large area of low atmospheric pressure which is connected to the North African low-pressure trough and a high-pressure area over eastern Africa. Winds in the Arabian Sea are from the southwest, changing to north-northwest in the southern part of the Red Sea. During the Northeast (NE) monsoon, there is a low-pressure field over eastern Africa and high-pressure areas over central Asia and northern Africa. Winds over the Arabian Sea are northeasterly, changing to south-southeasterly in the southern part of the Red Sea. In the northern Red Sea the prevailing wind is from north-northwest year-round (Siedler, 1969) (figure 1).

The NE monsoon directs water from the Arabian Sea into the Gulf of Aden, with continuing surface flow into the Red Sea through the Strait of Bab al Mandab. A general cyclonic flow results along the Red Sea coastline (figure 1). North of $20^{\circ}$ N, the average direction of the current is northwest, against the prevailing winds. As a result of this opposition, a convergence zone develops near $20^{\circ}$ N (Halim, 1984). During the NE monsoon, the surface waters flow northerly, sink in the northern Red Sea, then return south as a warm, high-salinity, subsurface current that flows out over the shallow sill into the Gulf of Aden (Patzert, 1974) (figure 2). Cold, low-salinity water in the Gulf of Aden, apparently due to seasonal upwelling of deep Arabian Sea water along the southern coast of Arabia, flows over the sill and mixes with Red Sea surface water (Jones and Browning, 1971).

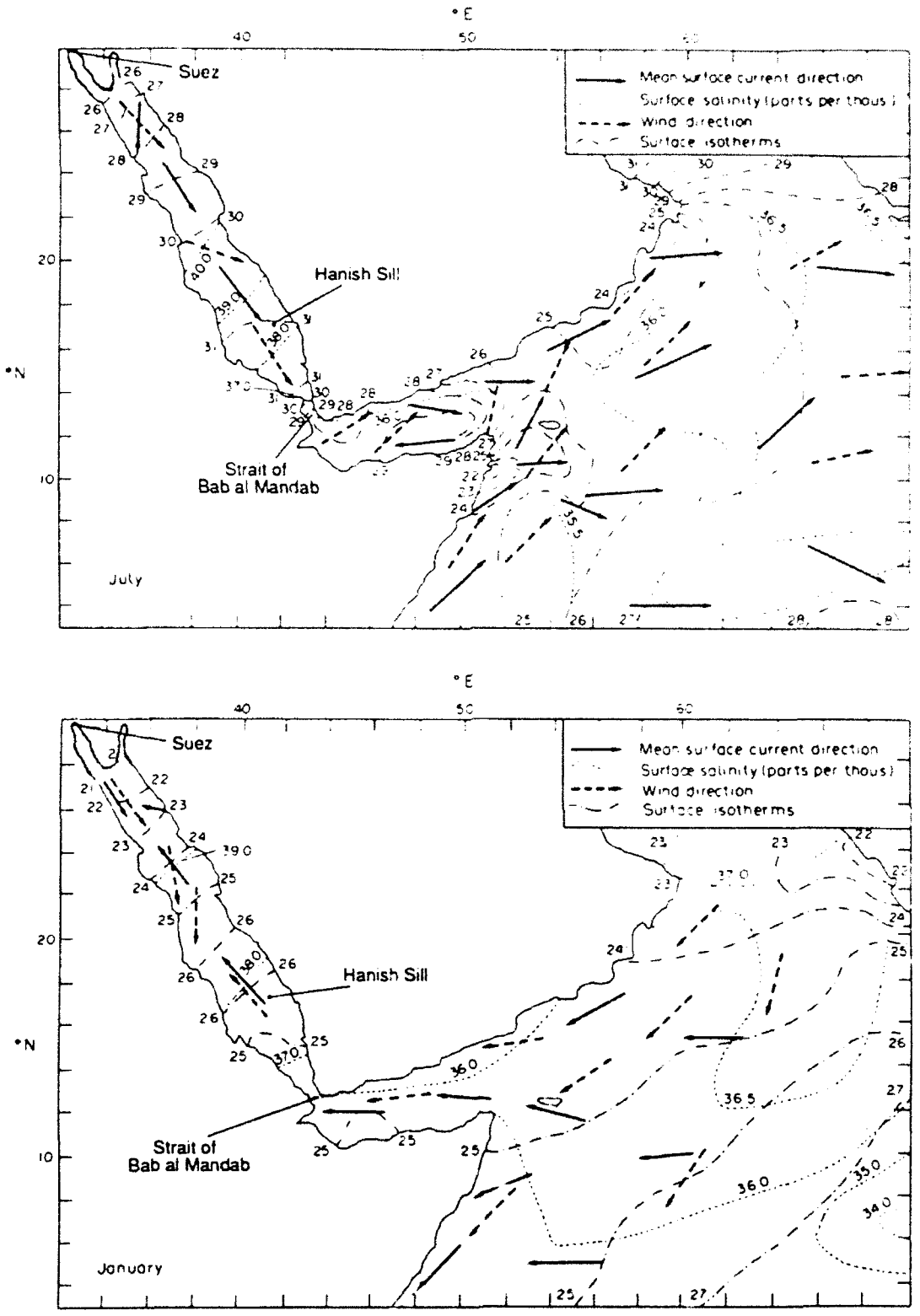


Figure 1. Mean Surface Current Direction and Wind Direction for July and January (Halim, 1984).

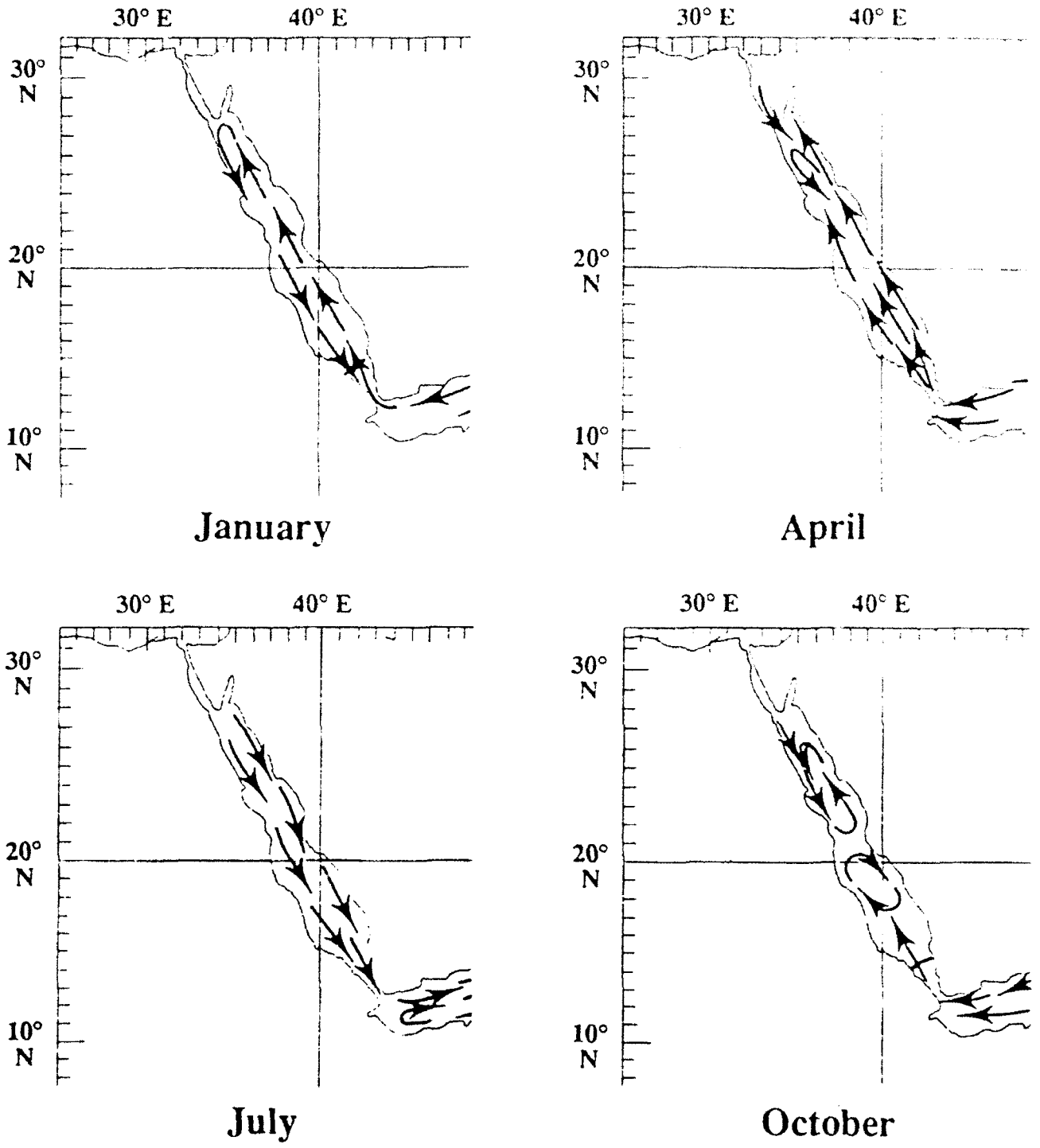


Figure 2. Surface Current Patterns in the Red Sea for January and July and the Transition Months of April and October (Naval Weather Service Detachment, 1976).

During the SW monsoon, the direction of the surface transport is south-southeast down the Red Sea Basin. South of 20° N, the currents are slightly stronger in the vicinity of the Strait of Bab al Mandab. At this point, the surface water of the Gulf of Aden flows into the Arabian Sea as an easterly current and is replaced by water flowing from the Red Sea through the Strait of Bab al Mandab (figures 1 and 2) (Morcos, 1970). During the SW monsoon, the wind stress and thermohaline forces have opposite effects. Three water masses are observed: (1) a surface layer (at 40 m) that is outflowing, (2) a layer of deep Red Sea water outflowing over the sill, and (3) a layer of Gulf of Aden water inflowing between these two layers.

The monsoonal transition periods occur when the winds reverse direction. Transitional months are April and October (figure 2). The mean monthly currents are weakest and most variable during transitional periods (Patzert, 1974). There is also little or no flow through the Strait of Bab al Mandab during transitional periods (Morcos, 1970).

## III. OPTICAL PROPERTIES FROM CZCS

The ocean color imagery gathered by CZCS was used to determine monthly climatological diffuse attenuation coefficients from January 1979 to December 1980. This period extended through one complete NE monsoon and two complete SW monsoons. The NE monsoon begins in October, peaks in January, and extends through April. The SW monsoon commences in May, peaks in July, and continues through September.

The CZCS collected approximately 66,000 2-minute scenes of high-spectral resolution ocean color data from November 1978 to June 1986. The CZCS was a multichannel scanning radiometer using a rotating plane mirror at a 45-degree angle to the optic axis of a Cassegrain telescope (Hovis et al., 1980). The rotating mirror scans 360 degrees; however, only 80 degrees of data centered on the spacecraft nadir are collected for ocean color measurements at a ground resolution of approximately 800 m at nadir. The CZCS had six spectral bands: five sensing backscattered solar radiance and one sensing emitted thermal radiance. The channels were selected to cover specific narrow chlorophyll absorption bands and were designed to measure subtle ocean color signatures.

The level 1 CZCS data represent the "raw" data that are uncalibrated and uncorrected for atmospheric contamination. Level 2 products determine the ocean color and water leaving radiance by removal of the atmospheric contamination. The atmospheric signal contributes approximately 80 to 90 percent of the total signal sensed at the satellite. The National Aeronautics and Space Administration (NASA) Goddard Space Flight Center (GSFC) processed the 66,000 2-minute scenes, using the atmospheric correction of Gordon and Clark (1980) for water leaving radiances at 443, 520, and 550 nm. This processing assumes the

670-nm channel represents the aerosol path radiance and further assumes a constant character to the aerosol distribution (Angstrom coefficient = 0) (Feldman et al., 1989; Gordon and Clark, 1980; Arnone and Oriol, 1990a). GSFC composites of CZCS imagery generated level 2 and level 3 registered products of monthly averages of the normalized water leaving radiances (443, 520, and 550 nm) at a spatial resolution of 20 km. This was performed by taking full-resolution CZCS imagery (1 km) and a spatial averaging of approximately 400 pixels from individual scenes to obtain an average 20-km pixel. Additionally, the global CZCS database further assumes a temporal averaging by collecting all spatially averaged scenes from a 1-month period and again averaging. There are inherent sampling problems resulting from inconsistent data coverage, which are recognized (Arnone and LaViolette, 1991; Abbott and Zion, 1985; and Chelton and Schlax, 1991). The global database produced a monthly mean water leaving radiance for the entire life of the CZCS sensor.

The CZCS ocean color data represent water leaving radiance within the surface layer, i.e., the first attenuation length, 1/K, (Gordon and McCluney, 1975). The determination of the diffuse attenuation coefficient, K, at 490 nm can be computed from the ratio of water leaving radiances derived from the CZCS ocean color data (Austin and Petzold, 1981; Mueller et al., 1990). The value of K(490) is a measure of the rate in which visible radiation is attenuated in the surface ocean. Typically, the subsurface vertical K(490) distribution can be considerably different than the surface value (Kitchen and Zaneveld, 1990); however, the surface distribution provides a realistic estimate of the surface optical climatology. An optical climatological database has been constructed based on the water leaving radiances from GSFC processing of CZCS data (Arnone et al., 1990b). These data have been combined and assembled on Write-Once-Read-Many (WORM) optical disk. The database was constructed using PC-SEAPAK software (Firestone et al., 1989; McClain et al., 1990), and all processing used in generating the statistics was compiled using PC-SEAPAK. Optical data from this database were used in determining statistics of the Red Sea.

The monthly average K(490) distribution from January 1979 to December 1980 was used to derive statistics of the optical character of the Red Sea. Six provinces were chosen which represent significantly different ocean regimes from which statistics were derived (figure 3). Waters entering the Gulf of Aden at the Strait of Bab al Mandab are less dense (lower salinity) than resident Red Sea waters. As these lower salinity waters mix, they move northward and sink because of high evaporation and cooling (Poisson et al., 1984). The northern region of the Red Sea represents an elevated salinity of approximately 40 ppt (Siedler, 1969). The changing salinity character formed by the mixing of Gulf of Aden water and high-salinity subsurface water has been used to segment provinces within the Red Sea. The mixing processes at the surface are controlled by both geostrophic circulation and surface wind stress. This physical forcing

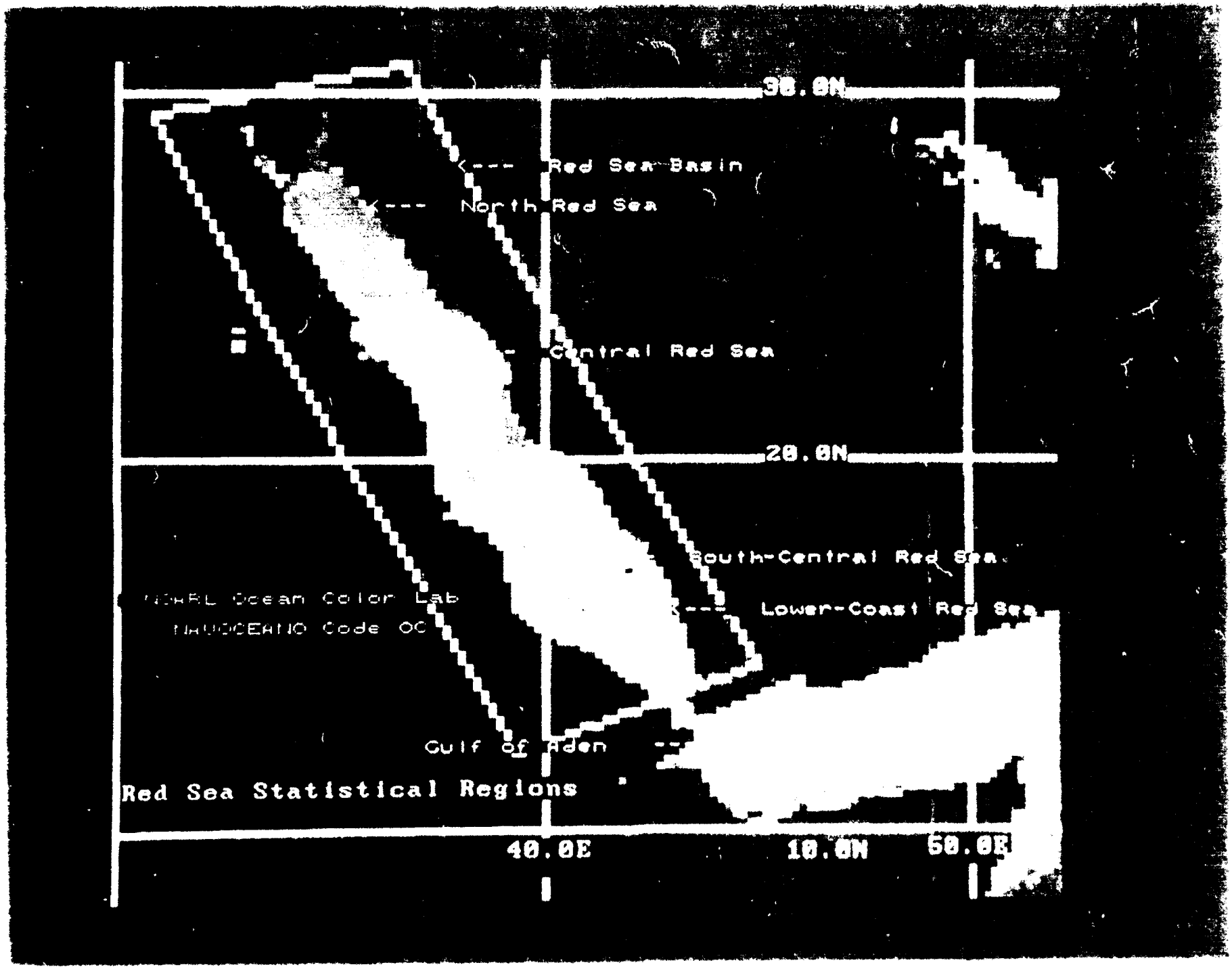
30.0N
1
<--- Red Sea Basin
<--- North Red Sea
- Central Red Sea
20.0N
South-Central Red Sea
NASA Ocean Color Lab
NAVOCEANO Code OC
<--- Lower-Coast Red Sea
Gulf of Aden --
Red Sea Statistical Regions
40.0E
10.0N
50.0E

results in water-mass mixing and is believed responsible for controlling the optical signatures observed in the following provinces:

(1) Northern Red Sea (3700 sq km): represents the deep-water, high-salinity area of the basin where upwelling occurs in October (Poisson et al., 1984) and is characterized by hot brine pools and a reduction in biological activity below 1100 m (Gideiri, 1984). Bottom water is formed during the winter season in the Northern Red Sea (Morcos, 1970).

(2) Central Red Sea (5340 sq km): represents the transition area where Gulf of Aden surface water begins to "pile up" at approximately 20° N and then sinks below the Red Sea resident waters.

(3) South Central Red Sea (2140 sq km): represents the area of increased variability caused by the less dense Gulf of Aden waters entering the Strait of Bab al Mandab and mixing with the resident denser waters of the Red Sea.

(4) Lower Coastal Red Sea (5560 sq km): represents biologically rich waters resulting from upwelling of deep water near the Hanish Sill (Cember, 1988). This relatively shallow area has multiple coral reefs along the coast.

(5) Gulf of Aden (3700 sq km): characterized by less dense waters with salinities less than 37 ppt and cooler temperatures (18 °C), which result from cooler, monsoon-driven, upwelled Arabian Sea water.

(6) Total Red Sea (26,800 sq km): represents a composite region from which different provinces will be compared to determine each region's contribution.

## IV. RESULTS

The monthly CZCS composite of K(490) are shown in figures 4 through 10. These images, representing January 1979 to December 1980, have been registered to an equirectangular projection and pseudocolored to represent the optical property distribution. The K(490) color scale that appears in figures 4 and 10 applies to the entire sequence.

During the NE monsoon (November), pelagic organisms enter the Red Sea from the Gulf of Aden and diffuse northward through the Red Sea Basin (Halim, 1984). Observed optical properties of the Red Sea obtained from CZCS indicate a similar biological productivity decrease from south to north. There is a slight increase in the value of K(490) for all regions of the Red Sea during the NE monsoon (November to April) compared to the SW monsoon (May to October).

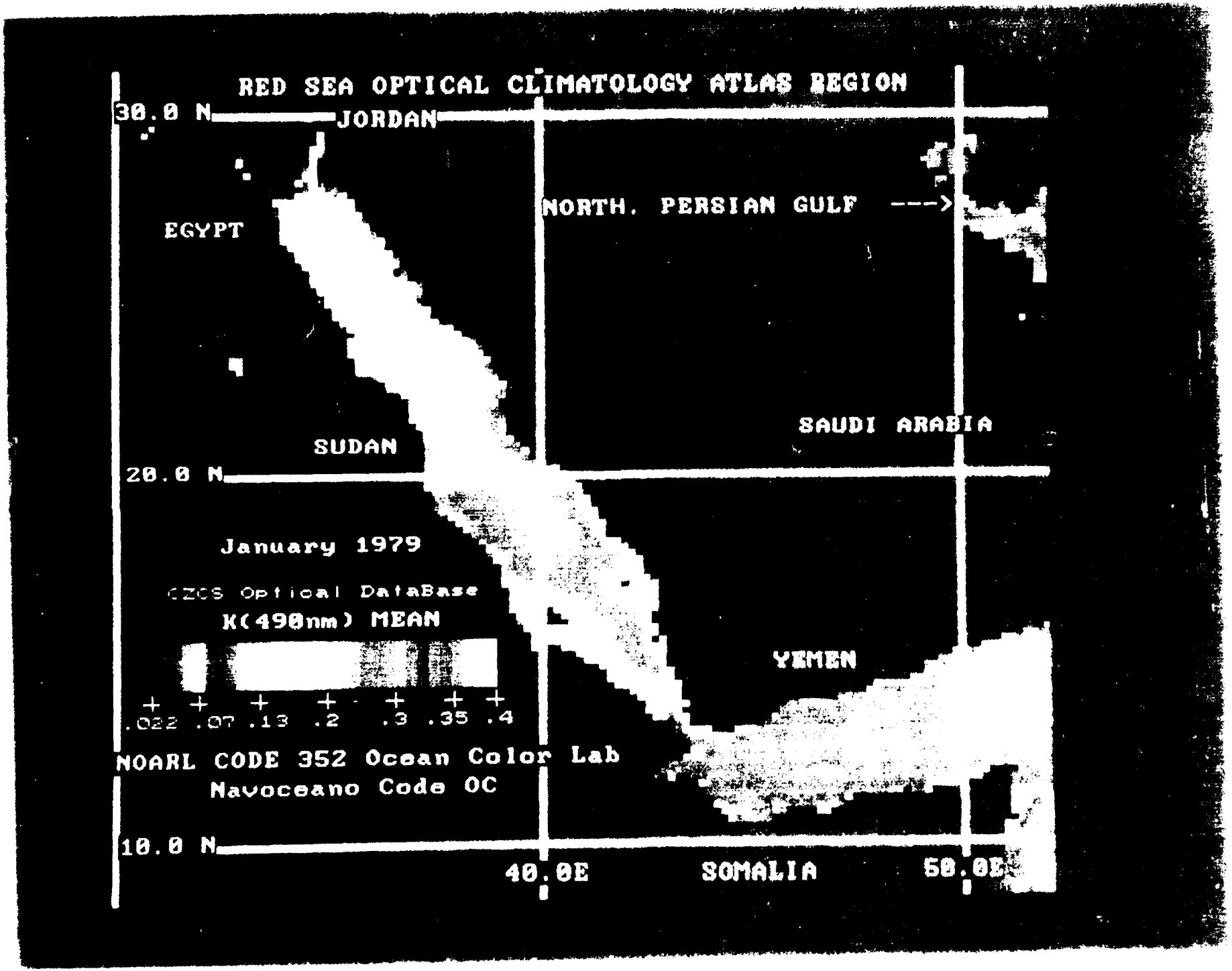
RED SEA OPTICAL CLIMATOLOGY ATLAS REGION
30.0 N
JORDAN
NORTH. PERSIAN GULF --->
EGYPT
SAUDI ARABIA
SUDAN
20.0 N
January 1979
CZCS Optical DataBase
K(490nm) MEAN
.022 .07 .13 .2 .3 .35 .4
YEMEN
NOARL CODE 352 Ocean Color Lab
Navoceano Code OC
10.0 N
40.0E
SOMALIA
50.0E

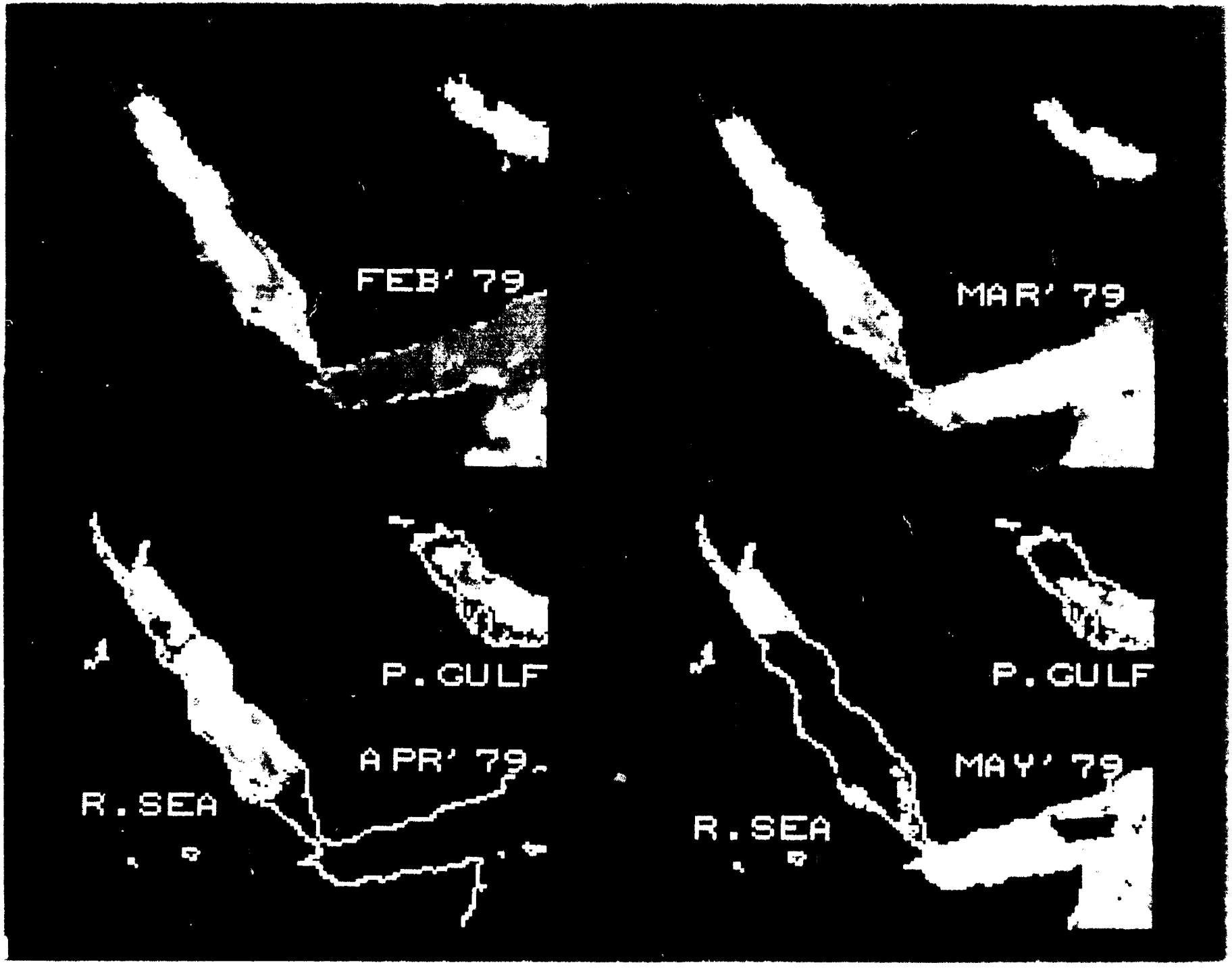
FEB' 79
MAR' 79
P. GULF
P. GULF
APR' 79
MAY' 79
R. SEA
R. SEA

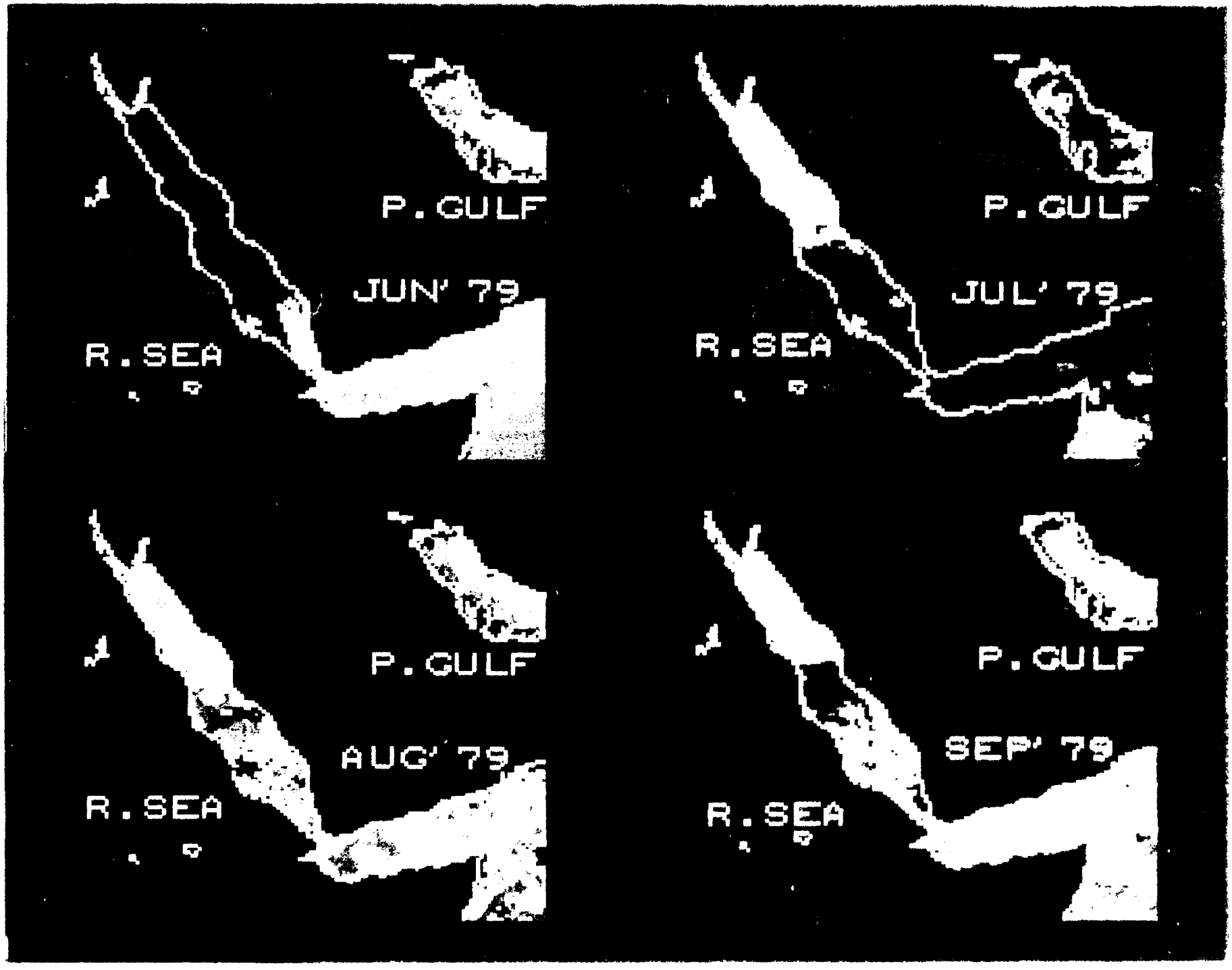
P. GULF
JUN' 79
R. SEA
P. GULF
JUL' 79
R. SEA
P. GULF
AUG' 79
R. SEA
P. GULF
SEP' 79
R. SEA

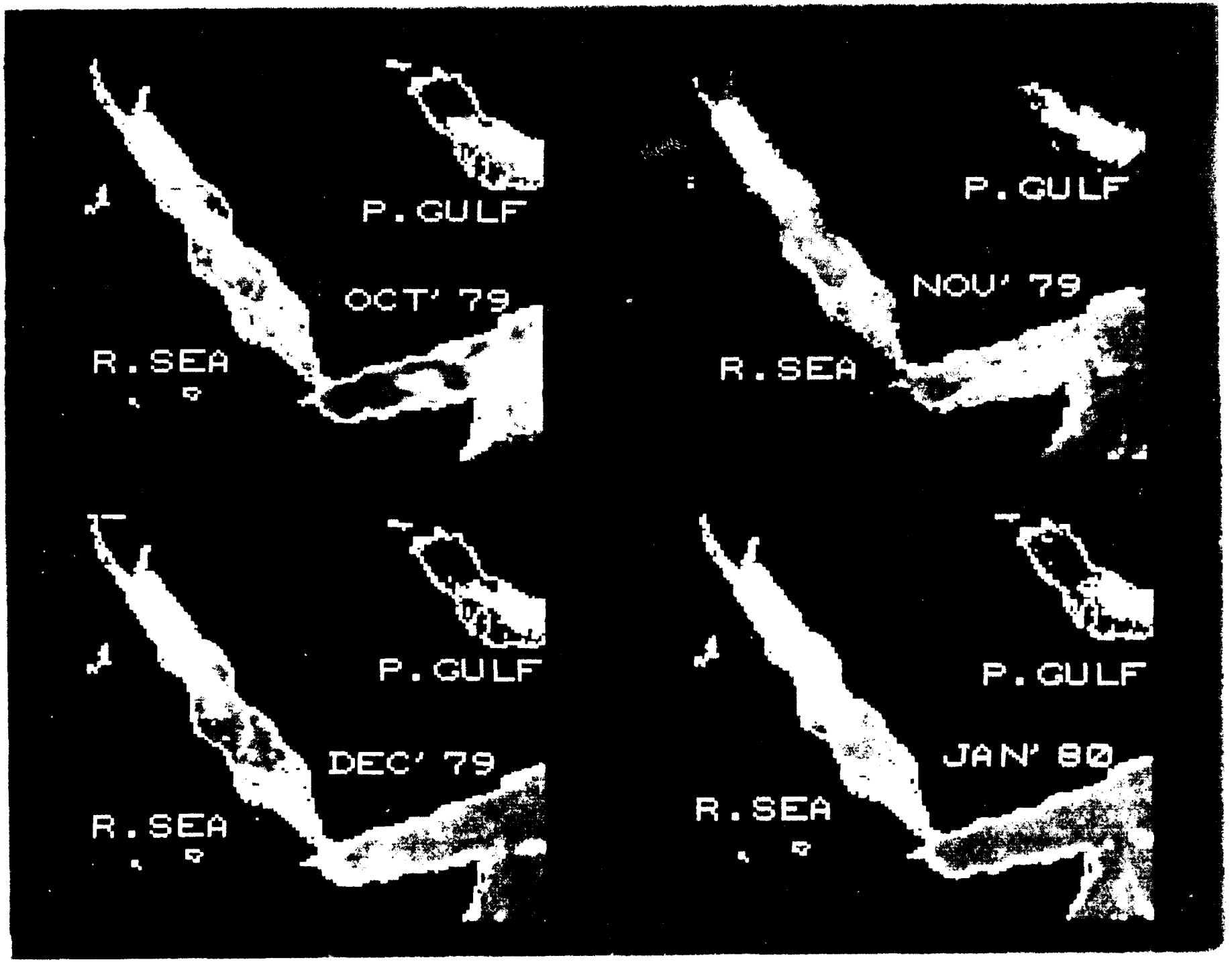
P. GULF
OCT' 79
R. SEA
P. GULF
NOV' 79
R. SEA
P. GULF
DEC' 79
R. SEA
P. GULF
JAN' 80
R. SEA

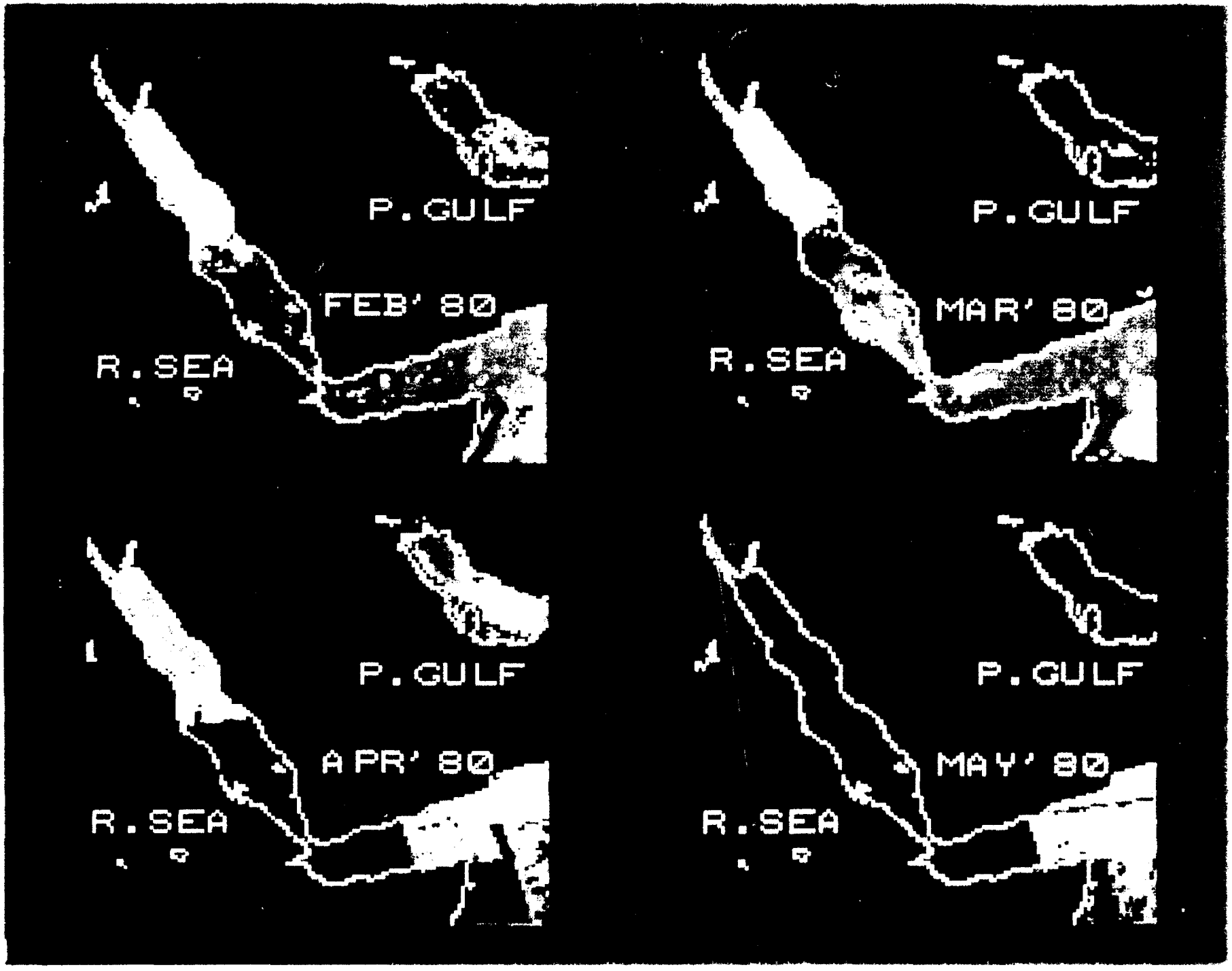
P. GULF
FEB' 80
R. SEA
P. GULF
MAR' 80
R. SEA
P. GULF
APR' 80
R. SEA
P. GULF
MAY' 80
R. SEA

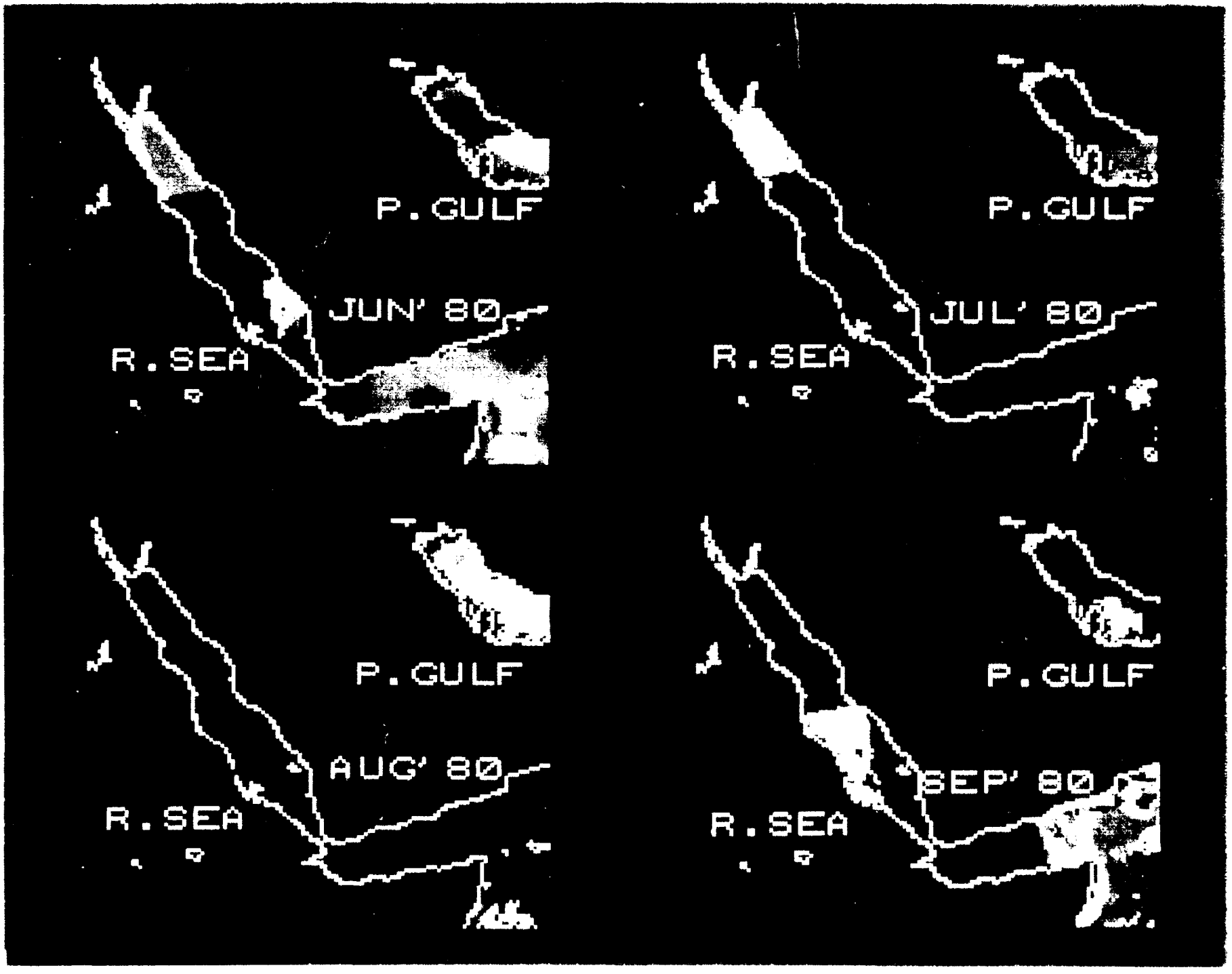
P. GULF
JUN' 80
R. SEA
P. GULF
JUL' 80
R. SEA
P. GULF
AUG' 80
R. SEA
P. GULF
SEP' 80
R. SEA

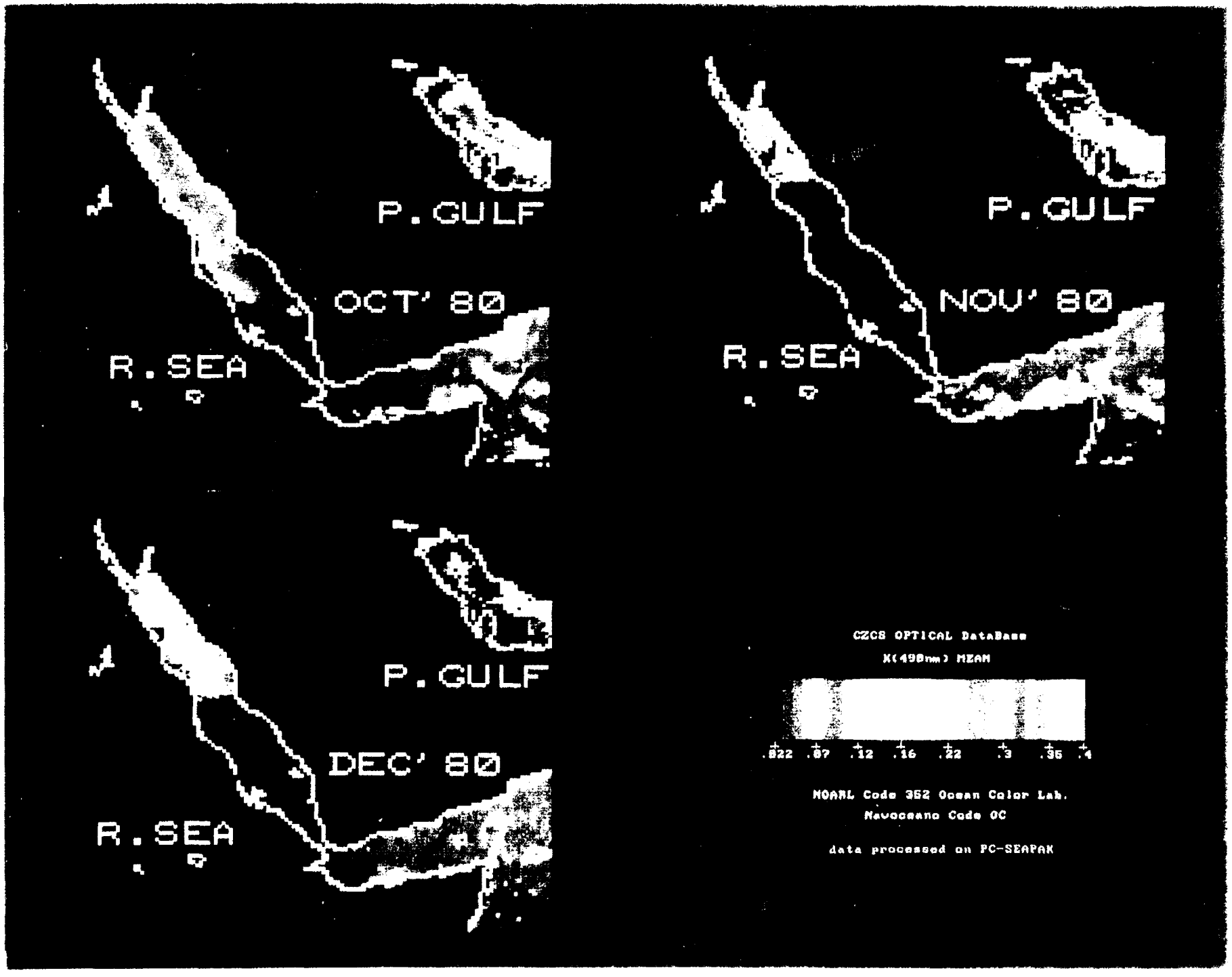
P.GULF
OCT' 80
R.SEA
P.GULF
NOV' 80
R.SEA
P.GULF
DEC' 80
R.SEA
CZCS OPTICAL DataBase
X(490nm) MEAN
.822 .87 .12 .16 .22 .3 .35 .4
NOAAL Code 352 Ocean Color Lab.
Navoceano Code OC
data processed on PC-SEAPAK

The statistics of the K(490) distribution in the six regions obtained from the CZCS data are displayed in figures 11 through 16. The mean monthly K(490) values for 1979 and 1980 and the interannual differences are depicted on these regional plots. The standard deviation is also shown.

In the Northern Red Sea, K(490) remains relatively constant, with values ranging from 0.030 to 0.036 (figure 11). North of 20° N, the Red Sea is considered oligotrophic as a result of reduced nutrients (Auras-Schudnagias et al., 1989) and low biological activity. This area does not show any seasonal trend and similarly has a low standard deviation of approximately 0.05. The monsoon season has minimal influence on this region's optical properties.

The Central Red Sea (figure 12) remains relatively constant, with K(490) ranging from 0.0288 to 0.0381. This region is characterized by low K(490) values, suggesting low biological activity. A modest increase in K(490) of 0.035 is observed in September. There is also an increase in variability, which suggests a slight response to the monsoon season.

The K(490) values in the South Central Red Sea are slightly higher (0.0350 to 0.0476) than the Central Red Sea region (figure 13). A seasonal response is observed with the lowest values occurring during the SW monsoon and the highest values occurring during the NE monsoon.

The Lower Coastal Red Sea is an area of high biological activity where 95 percent of the zooplankton biomass is located in the upper 100 m (Halim, 1984). Elevated K(490) values are observed in the lower coastal region (figure 14). These values range from 0.0496 to 0.1532 for 1979 to 1980 and correspond to the shallow waters of the coral reef zone (figure 1). This region similarly shows the greatest optical variability. The lowest values occur during the SW monsoon and the highest values occur at the onset of the NE monsoon.

The comparison of average K(490) for each Red Sea region to the Total Red Sea is shown in table I. Average K(490) values listed in the table represent the average for each month over the period of 1979 to 1980. The values represent a percentage above or below the Total Red Sea average of 100 percent. To calculate this, the average ($K_1$) per region was divided by the mean ($K_T$) of the Total Red Sea and multiplied by 100 ($K_1/K_T \times 100$). For example, in November the Lower Coastal Red Sea region had a mean K(490) 65 percent greater than the average K(490) of the Total Red Sea. Similarly, the Northern Red Sea region in September had an average K(490) 45 percent lower than the average for the entire Red Sea K(490).

The Lower Coastal Red Sea region had significantly higher K(490) than the average Total Red Sea for all months. This region elevated the Total Red Sea average. The other regions

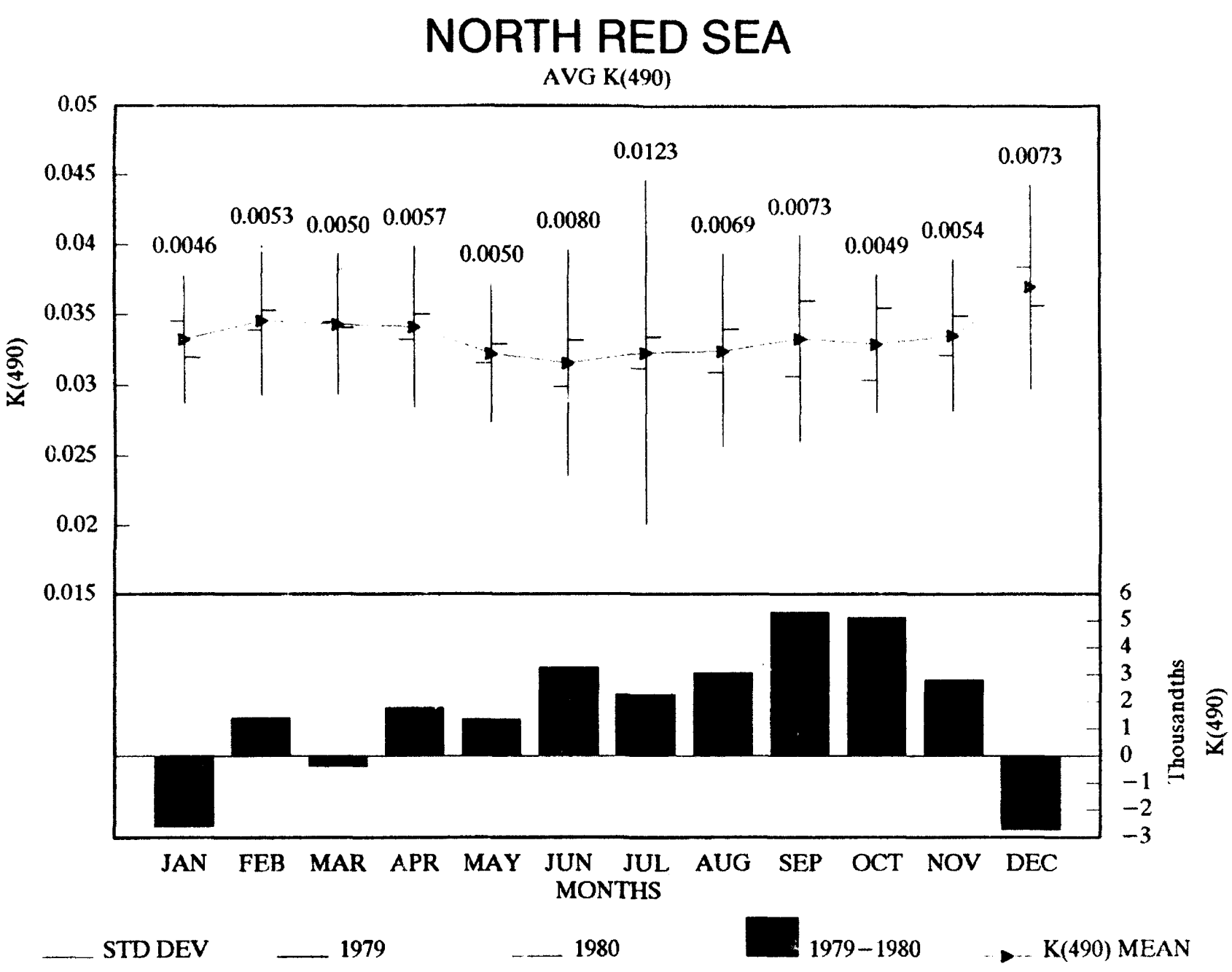


Figure 11. North Red Sea Mean Monthly K(490) Values for 1979-1980 and the Standard Deviation for 12 Months.

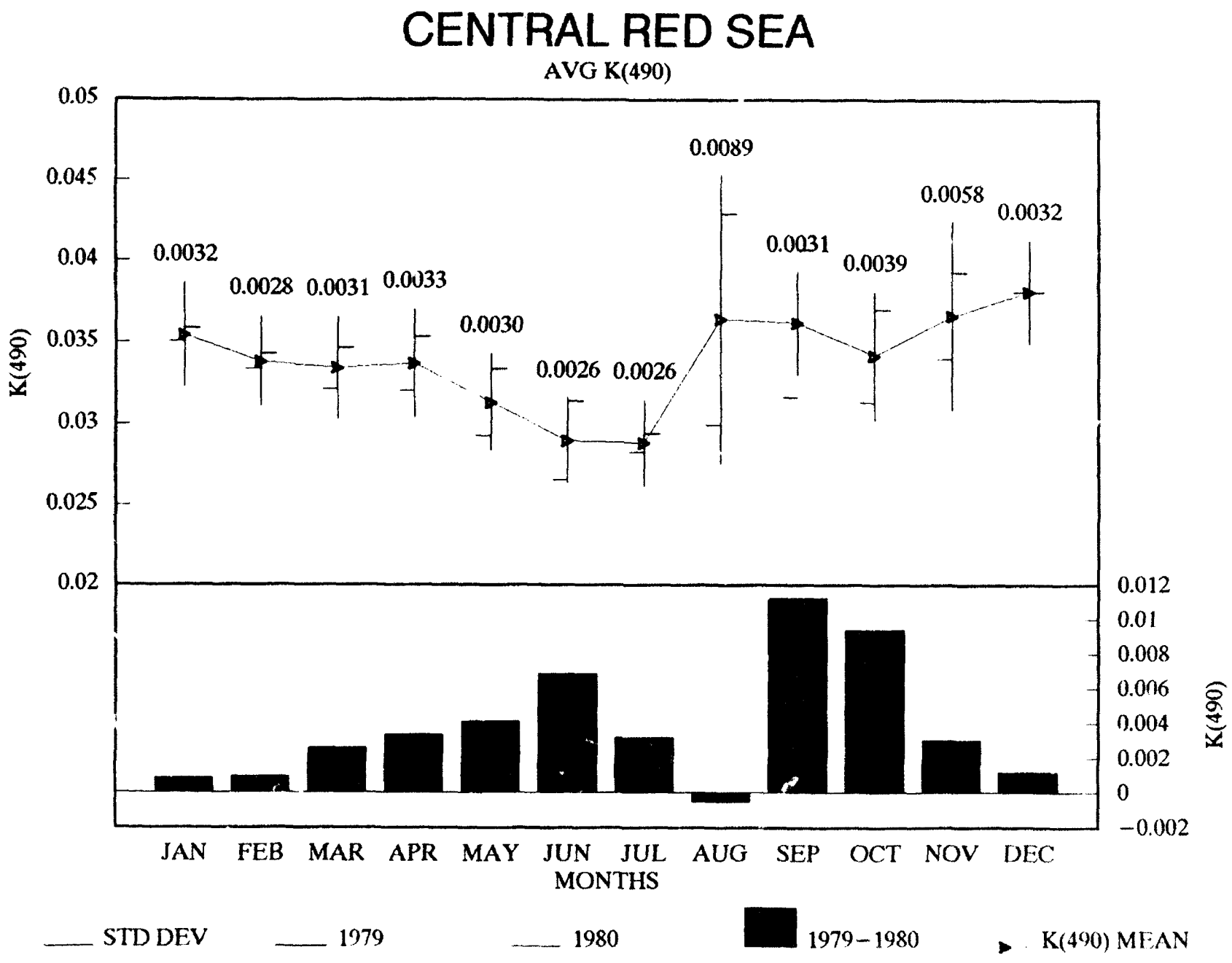


Figure 12. Central Red Sea Mean Monthly K(490) Values
1980 and the Standard Deviation for 12 Mo

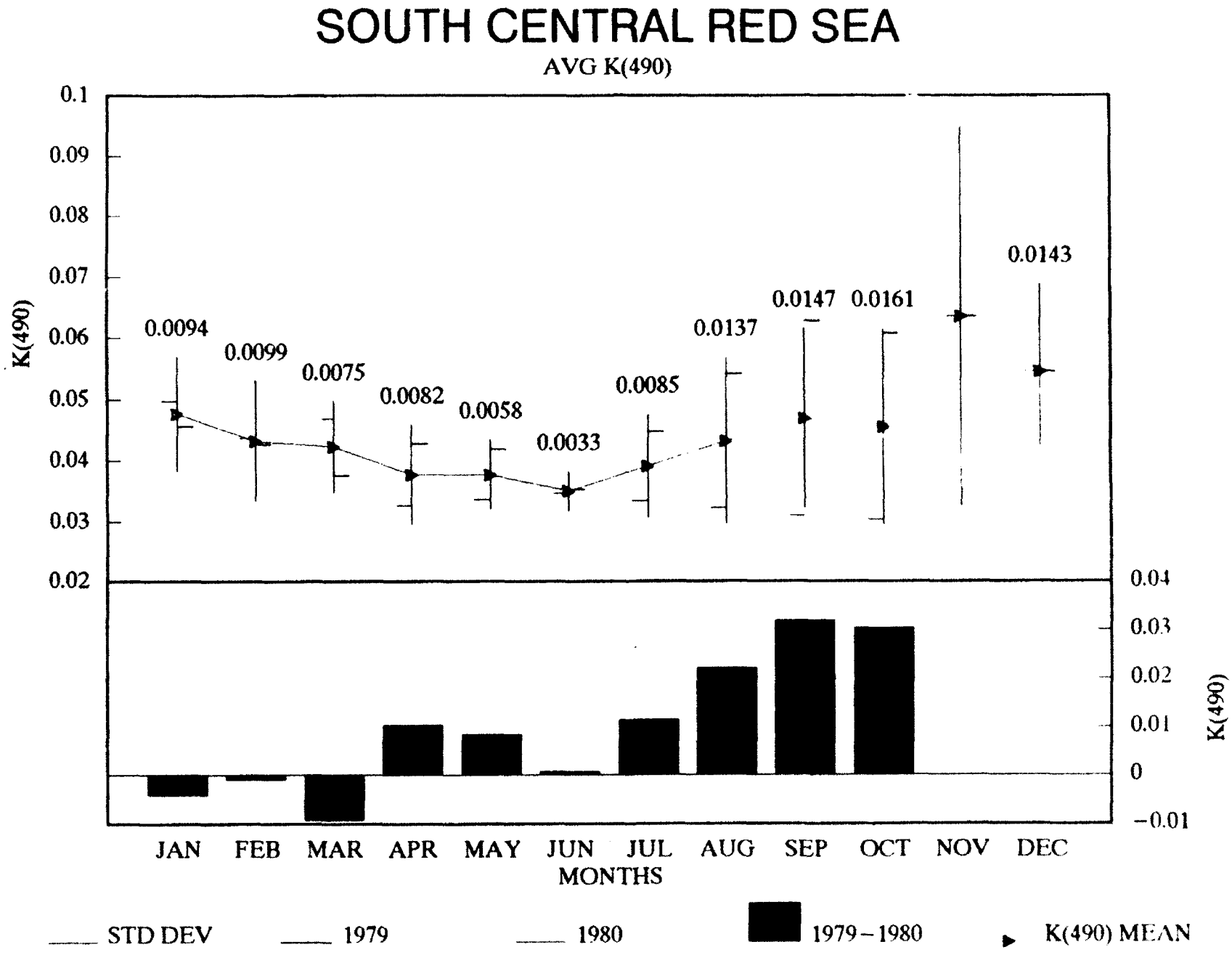


Figure 13. South Central Red Sea Mean Monthly K(490) Values for 1979-1980 and the Standard Deviation for 12 Months.

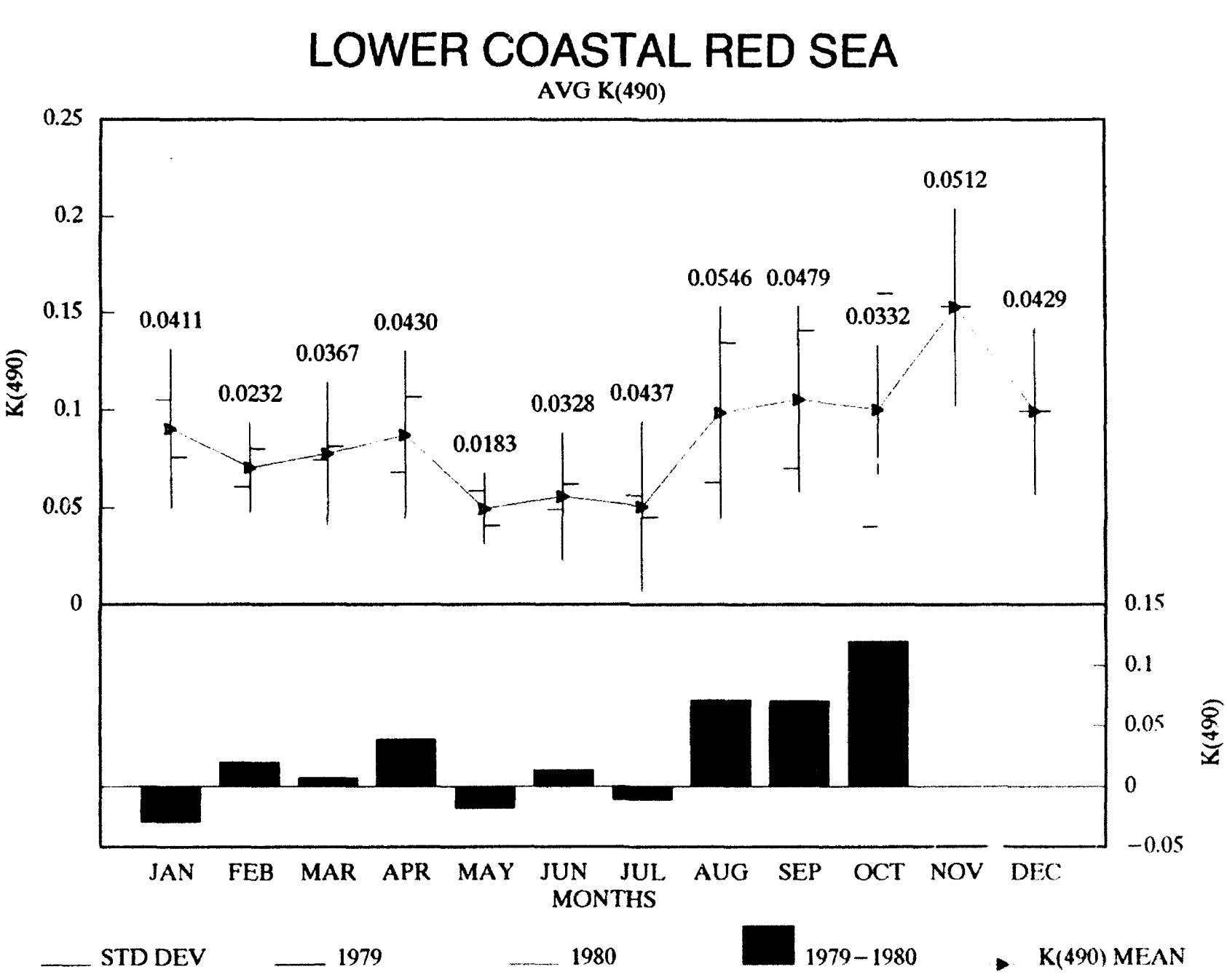


Figure 14. Lower Coastal Red Sea Mean Monthly K(490) Values for 1979-1980 and the Standard Deviation for 12 Months.

Table I. Comparison of Average K(490) Per Region to Average K(490) of Total Red Sea.

| | North | Central | South Central | Lower Coastal | Total |
|---|---|---|---|---|---|
| Jan | 60.8949 | 64.8485 | 87.1526 | 165.4668 | 100.0 |
| Feb | 77.4987 | 76.7236 | 96.6592 | 157.6150 | 100.0 |
| Mar | 69.6522 | 70.3804 | 85.7810 | 157.7709 | 100.0 |
| Apr | 76.1832 | 78.8182 | 84.0334 | 194.7476 | 100.0 |
| May | 89.2629 | 92.2727 | 104.3382 | 137.1827 | 100.0 |
| Jun | 68.5058 | 68.1009 | 75.8909 | 120.7068 | 100.0 |
| Jul | 92.9512 | 84.5732 | 112.3467 | 145.2791 | 100.0 |
| Aug | 57.9743 | 76.6274 | 77.0918 | 176.4385 | 100.0 |
| Sep | 55.0645 | 67.2525 | 77.5260 | 174.4718 | 100.0 |
| Oct | 58.7955 | 66.0000 | 81.2233 | 178.6783 | 100.0 |
| Nov | 57.9848 | 67.8689 | 109.7960 | 264.4776 | 100.0 |
| Dec | 72.4050 | 74.5525 | 106.7315 | 194.3765 | 100.0 |

were substantially lower than the average. The Lower Coastal Red Sea region exhibited the greatest variability for the 2-year period, which reflects higher biological activity around the coastal areas and coral reef zones. Table I shows that the Lower Coastal Red Sea has consistently higher K(490) compared to the average. This is followed by the South Central Red Sea region, which has K(490) close to the average. The Central Red Sea and Northern Red Sea regions have lower K(490) than the average.

According to table I, the percentage of contribution in the Lower Coastal Red Sea increases markedly in November, which is the onset of the NE monsoon. At this time, cooler water is flowing into the Lower Coastal Red Sea from the Gulf of Aden (Jones and Browning, 1971), causing increased productivity and higher K(490). Northern Red Sea values are highest in July, which corresponds to the peak of the SW monsoon. During this monsoon, deep water is upwelled in the Northern Red Sea due to prevailing north-northwesterly winds (Siedler, 1969). The South Central Red Sea also has a greater contribution (12 percent over total average) during July. This can be explained by the convergence zone that develops near $20^{\circ}$ N as a result of the average northwest current direction and opposing south-southeasterly winds (Halim, 1984). The Central Red Sea average contribution remains basically consistent for the 2-year period.

The Total Red Sea region (figure 15) has a high standard deviation, resulting from different optical regimes, and a range of K(490) from 0.0348 to 0.0605. The highest K(490) values are observed in August, September, and November. The greatest variability occurs at the beginning of the NE monsoon (November) as the biological activity responds to strong mixing. The bar graph at the bottom of figure 15 shows that the 1979 optical data was substantially greater than the 1980 data. These interannual changes are perhaps related to the strength of the monsoons and account for the high standard deviation observed.

Values of K(490) in the Gulf of Aden range from 0.0286 to 0.0602. The Gulf of Aden region (figure 16) has a strong seasonal response to the monsoons. Low K(490) values are observed during the SW monsoon. An increase in K(490) is observed between October and November. The variability of K(490) ranges from 0.0286 in June to 0.0602 in December. The highest standard deviation is observed in August.

## V. CONCLUSIONS

The CZCS data can be used for determining optical characteristics of the Red Sea. The 24-month period selected from 1979 to 1980 demonstrated the variability in K(490). The K(490) changes observed in the Red Sea are believed to be coupled with the seasonal effects of the monsoons. The Northern and Central Red Sea regions exhibited low variability and appeared to be influenced minimally by the monsoons. The Southern Red Sea

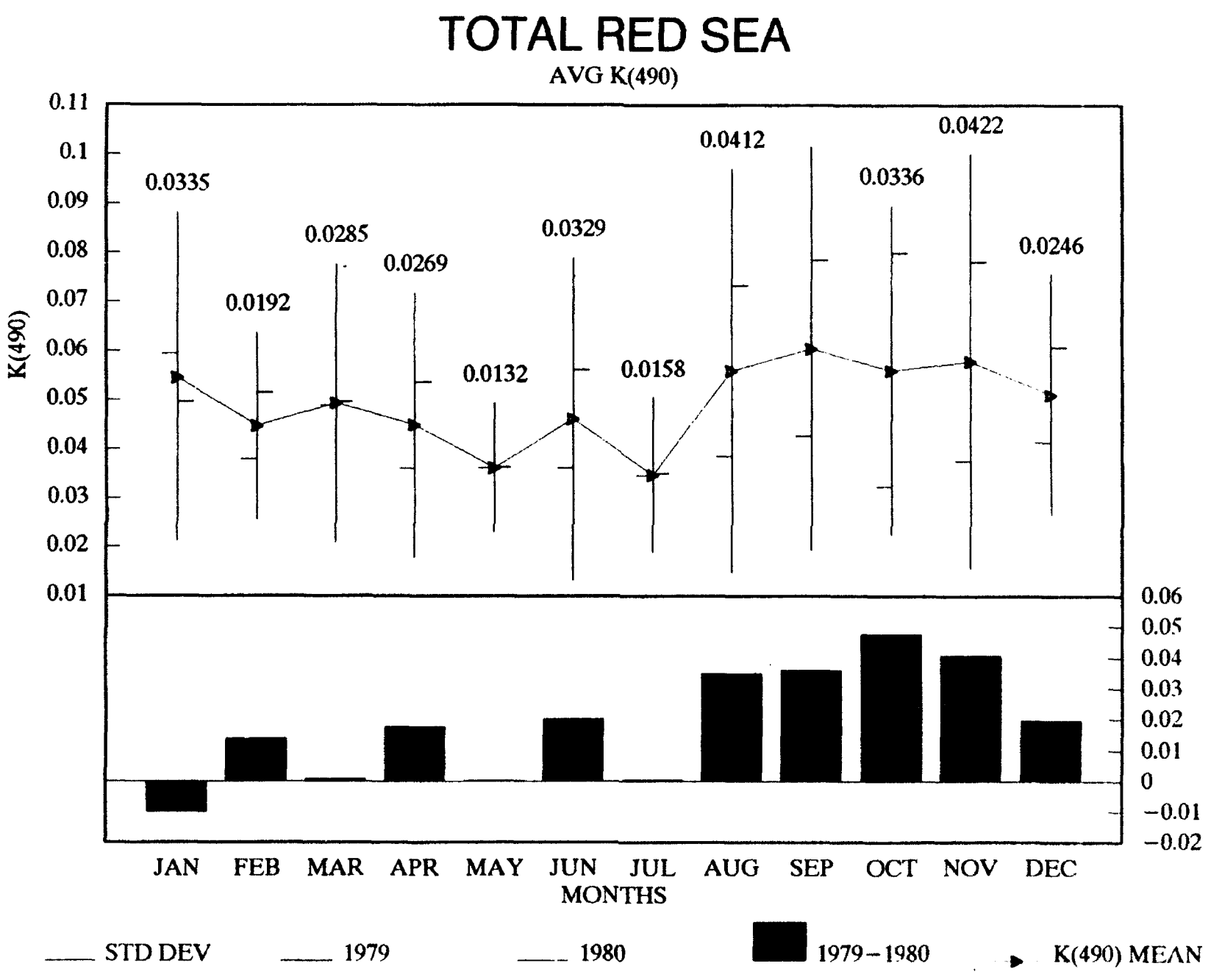


Figure 15. Total Red Sea Mean Monthly K(490) Values for 1979-1980 and the Standard Deviation for 12 Months.

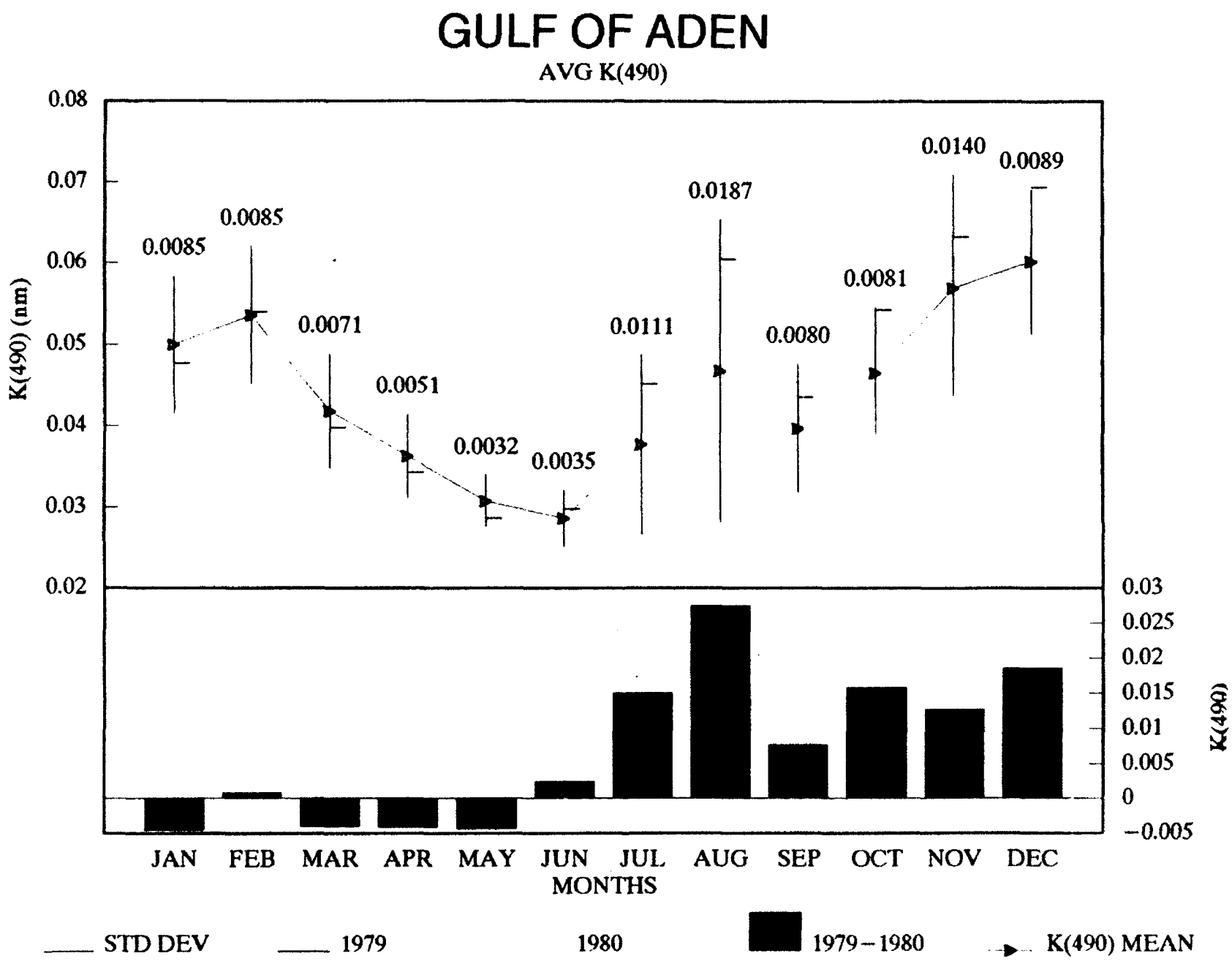


Figure 16. Gulf of Aden Mean Monthly K(490) Values for 1979-1980 and the Standard Deviation for 12 Months.

exhibited moderate variability. The Lower Coastal Red Sea had the greatest variability. Both southern regions appeared to be closely coupled to monsoonal influence.

The 1979 and 1980 data showed considerable differences in K(490) values on a monthly scale. The interannual variability observed in 2 years indicated that a doubling of K(490) can occur. This suggested that local seasonal events responding to changing monsoonal conditions has significant impact on predicting the optical environment. To more properly represent the average optical environment in the Red Sea, statistics must be gathered from a larger data set, which would entail the use of the entire 6-year CZCS data set.

## VI. REFERENCES


Abbott, M.R., and P.M. Zion; Satellite Observations of Phytoplankton Variability During an Upwelling Event, Continental Shelf Research, 1985, 4: 661-680.

Arnone, R.A., and P.E. LaViolette; A Methodology to Determine the Ocean Biological Climatology Using Regional Data Base Models, International Leige Colloquium on Ocean Hydrodynamics, 1991.

Arnone, R.A., and R.A. Oriol; Bottom Reflectance Discrimination Using Water Leaving Radiance from the Coastal Zone Color Scanner, Proceedings of the SPIE Ocean Optics X, Orlando, FL, 1990a, 1302: 612-623.

Arnone, R.A., R.A. Oriol, C.C. Trees, and J.L. Mueller; Bottom Reflectance Discrimination Using Water Leaving Radiance from the Coastal Zone Color Scanner, Proceedings of the SPIE Ocean Optics X, Orlando, FL, 1990b, p. 1302.

Auras-Schudnagias, A., D. Kroon, G. Genssen, C. Hemleben, and J.E. Van Hinte; Distributional Pattern of Planktonic Foraminifers and Pteropods in Surface Waters and Top Core Sediments of the Red Sea and Adjacent Areas Controlled by the Monsoonal Regime and Other Ecological Factors, Deep Sea Research, 1989, 36(10): 1515-1533.

Austin, R.W., and T.J. Petzold; The Determination of the Diffuse Attenuation Coefficient from the Coastal Zone Color Scanner, Oceanography from Space, 1981, Plenum, New York.

Cember, Richard P.; On the Sources, Formation, and Circulation of Red Sea Deep Water, Journal of Geophysical Research, 1988, 93: 8175-8191.

Chelton, D.B., and M.G. Schlax; Estimation of Time Averages from Irregularly Spaced Observations with Application to CZCS Estimation of Chlorophyll Concentration, Journal of Geophysical Research, 1991, 96(C8): 14, 669-14, 692.

Feldman, G., N. Kuring, C. Ng, W. Elaias, C. McClain, J. Elrod, N. Maynard, D. Endres, R. Evans, J. Brown, S. Walsh, M. Carle, and G. Podesta; Ocean Color: Availability of the Global Data Set, EOS, 1989, 70(23): 634-641.

Firestone, J.K., G. Fu, and M. Darzi; PC-SEAPAK: A State of the Art Image Display and Analyses System for NASA's Oceanographic Research Program, Proceedings of the Fifth Interactive and Information Processing Systems for Meteorology, Hydrography and Oceanography, American Meterological Society, Anaheim, CA, 29 Jan - 3 Feb 1989.

Gideiri, Y.B.A.; Impacts of Mining on the Central Red Sea Environment. Deep Sea Research, 1984, 31: 823-828.

Gordon, H.R., and D.K. Clark; Atmospheric Effects in Remote Sensing of Phytoplankton Pigments, Boundary Layer Meteorology, 1980, 19: 299-313.

Gordon, H.R., and McCluney, W.R.; Estimation of the Depth of Sunlight Penetration in the Sea for Remote Sensing, Applied Optics, 1975, 14: 413-416.

Halim, Y.; Plankton of the Red Sea and Arabian Gulf, Deep Sea Research, 1984, 31: 969-982.

Hovis, W.A., D.K. Clark, F. Anderson, R.W. Austin, W.A. Wilson, E.I. Butler, D. Ball, H.R. Gordon, J.L. Mueller, S.F. El-Sayed, B. Sturm, R.C. Wrigley, and C. Yentsch; Nimbus-7 Coastal Zone Color Scanner: System Description and Initial Imagery, Science, 1980, 210(4465): 60-63.

Jones, E.N., and D.G. Browning; Cold Water Layer in the Southern Red Sea, Limnology and Oceanography, 1971, 16(3): 503-509.

Kitchen, J., and R. Zaneveld; On the Noncorrelation of the Vertical Structure of Light Scattering and Chlorophyll a in Case 1 Waters, Journal of Geophysical Research, 1990, 95(C11).

Lewis, M.R., N. Kuring, and C.S. Yentson; Global Patterns of Ocean Transparency: Implications for New Production of the Open Ocean, Journal of Geophysical Research, 1988, 93: 6347-6856.

McClain, C.R., G. Fu, M. Darzi, and J.K. Firestone; PC-SEAPAK User's Version 3.0, NASA/GSFC, 1990.

Morcos, S.A.; Physical and Chemical Oceanography of the Red Sea, Oceanogr. Mar. Biol. Ann. Rev., 1970, 8: 73-202.

Morel, A., and L. Prieur; Analysis of Variation in Ocean Color, Limnology and Oceanography, 1977, 22(4): 709-722.

Mueller, J.L., C.C. Trees, and R.A. Arnone; Evaluation of Coastal Zone Color Scanner Diffuse Attenuation Coefficient Algorithms for Application to Coastal Waters, Proceedings of the SPIE Ocean Optics x, 1990, 1302.

Naval Weather Service Detachment, Asheville, NC; U.S. Navy Marine Climatic Atlas of the World, Vol. III, 1976.

Poisson, A., S. Morcos, E. Souvermezoglou, A. Papaud, and A. Ivanoff; Some Aspects of Biogeochemical Cycles in the Red Sea with Special Reference to New Observations Made in the Summer of 1982, Deep Sea Research, 1984, 31: 707-718.

Patzert, W.C.; Wind-induced Reversal in Red Sea Circulation, 1984, Deep Sea Research, 1974, 21: 109-121.

Siedler, G.; General Circulation of the Water Masses in the Red Sea, Hot Brines and Recent Heavy Metal Deposits in the Red Sea, Springer-Verlag, New York, 1969, 131-137.

Yoder, J.A., C.R. McClain, J.O. Blanton, and L. Dey; Spatial Scales in CZCS-Chlorophyll Imagery of the Southeastern U.S. Continental Shelf, Limnology and Oceanography, 1987, 32: 929-941.

Technical Note 03-93

# Distribution List

| | |
|---|---|
| DTIC Code OCC | 2 |
| NAVOCEANO Code N22 | 30 |
| N4311 | 2 |
| N4312 | 34 |
| NRL DET STENNIS SPACE CENTER Code 7240 | 30 |
| University of Southern Mississippi (Dr. Scott Dinnel, Dr. Donald Redalje) | 2 |